MONTE CARLO DOSE VERFICATION OF AN X-RAY BEAM IN A VIRTUAL WATER™ PHANTOM

A Thesis
Presented to
The Academic Faculty

by

Virginia L. Maniquis

In Partial Fulfillment
of the Requirements for the Degree
Master of Science in the
George W. Woodruff School of Mechanical Engineering

Georgia Institute of Technology
May 2006

MONTE CARLO DOSE VERIFICATION OF AN X-RAY BEAM IN A VIRUTAL WATER™ PHANTOM

Approved by:

Dr. Cassiano de Oliveira, Advisor
School of Mechanical Engineering
Georgia Institute of Technology

Dr. Nolan E. Hertel
School of Mechanical Engineering
Georgia Institute of Technology

Dr. Tim Fox
School of Mechanical Engineering
Georgia Institute of Technology

Date Approved: April 7, 2006

ACKNOWLEDGEMENTS

After having lived almost 24 years under God's grace I have learned that God never gives us more than we can handle. I'd like to thank Him for His constant guidance and the blessings He has bestowed upon me in the form of my family and friends. I am eternally grateful for my family, especially my parents, for their unending love and support in all facets of my life. I'd also like to thank my brother for his support and kindness during my academic studies.

In the technical community, I would like to thank my advisor, Dr. Cassiano de Oliveira for both his faith in my capabilities and his support in my education. I would also like to thank Dr. Nolan E. Hertel for his selfless guidance and aid. You have been a second advisor to me and your good natured heart and cheerful character is exceedingly rare in this world, thank you. I'd also like to thank Dr. Tim Fox for his guidance in the field of medical physics and help during my thesis.

I would also like to thank my fellow students who have taught, guided and supported me throughout the development of my thesis, especially Eric Burgett for his MCNP expertise, Dwayne Blaylock, Zhonglu Wang and Xin Zhang for their sound advice and help.

I would also like to give a special thanks to Jeff Catinella for his extensive help in acquiring the impossible. I'd like to thankfully acknowledge Dr. Cho, Dr. Siebers, Dr. Goorley, Dr. Mohan and Dr. Vassiliev for their expert guidance in the field of medical physics and for taking the time to help a student despite their busy schedules. I greatly appreciate it.

And finally, I would like to thank Ryan Lorio. I cannot express in words how grateful I am for you. Thank you, for your generous and loving heart and for the joy you bring into my life. Thank God for you. Thank God for all of you.

TABLE OF CONTENTS

LIST OF TABLES

LIST OF FIGURES

SUMMARY

Monte Carlo (MC) methods are widely accepted as the most accurate technique for calculating dose distributions in radiation therapy physics. Simulating the particle transport through the treatment head of a linear accelerator utilizing a MC based code is both a widespread and practical approach to determining detailed clinical beam characteristics such as the energy, angular and spatial distribution of particles which are needed to properly quantify dose. One particular and versatile MC code, the Monte Carlo N-Particle (MCNP) radiation transport code, developed by Los Alamos National Laboratory, has been commonly used to model ionizing radiations for medical physics applications.

In this thesis, a Varian 2100C linear accelerator (linac) is modeled and the electron and photon transport through the primary components of the treatment head are simulated using MCNP Version 5_1.3. The 6 MV photon spectra was characterized in a standard 10 x 10 cm^2 field and subsequent dose calculations were made in a Virtual Water™ (VW) phantom. Energy fluence, percent depth dose and beam profile measurements were taken in a modeled VW phantom and the calculated data was compared to measured reference data. In addition, a human phantom was modeled for future dose calculations using the modeled linac.

The linac model created can incorporate different beam energies for determining the dose distribution of multiple beam treatments in phantoms for standard 6 MV plans. The adaptability of this MCNP model allows for any number of geometries and sources encountered in medical physics to be computed and applied with relative ease. Future

studies can involve adding complex multi-leaf collimator beam shaping and calculating the dose in human phantom models, which would serve as a basis for studies involving MCNP modeling for dose optimization in medical physics applications.

CHAPTER 1

INTRODUCTION

Cancer is the second leading cause of death in the United States accounting for 22.7% of deaths each year (ACS, 2006). In the past 5 decades the cancer mortality rate has only decreased by 2% and it is estimated that approximately 1 in ever 3 individuals will be diagnosed with cancer (ACS, 2006). Of those diagnosed, approximately 50-60% of them will be treated with radiation therapy at some time during their illness.

Radiation therapy is the treatment of cancer with ionizing radiation. The primary goal of radiation therapy is to maximize the dose to the tumor cells and minimize the exposure to the healthy tissue. Increase use of high energy photon and electron beams in radiation therapy has made it necessary to account for the electron transport for dosimetry and treatment planning purposes.

The Monte Carlo (MC) method is a statistical simulation technique whose particle transport capabilities have progressed into many different areas of application since its introduction in the 1940s (Verhaegen, 2003). Applications of MC techniques in medical physics, especially radiation therapy physics, have been discussed in numerous publications (Rogers and Bielajew, 1990; Andreo, P., 1990; Ma et al., 1998) and have been demonstrated and accepted as the most accurate method for radiotherapy dose calculations.

In order to apply MC methods clinically, detailed information on beam particle characteristics such as energy, angular and spatial distributions is needed. One way to determine the essential clinical beam characteristics is to utilize the MC technique to simulate transport of particles through the treatment head of the linear accelerator (linac)

(Ma et al., 1998). For radiation transport problems, the MC method simulates individual particle tracks by sampling proper quantities from the probability distributions governing the individual physical processes using machine-generated pseudo-random numbers (Ma et al., 1999). By simulating a large number of particle histories, the particle fluence, energy spectrum and dose distribution can be computed.

Monte Carlo methods have been previously used to simulate particle transport of clinical photon and electron beams. A variety of research has been dedicated to modeling clinical beams and developing MC based codes for radiation therapy purposes. More specifically, there has been documented research done using the Los Alamos developed Monte Carlo N-Particle (MCNP) radiation transport code for simulating particle transport and modeling the key components of a treatment head to acquire energy and spectral distributions for various radiotherapy clinical beams (R.D. Lewis et al., 1999).

This thesis models a Varian 2100C* linac using MCNP5_1.3 to characterize the 6 MV photon spectra in a 10 x 10 cm^2 standard field size at 100 cm source-to-surface distance (SSD) to determine the dose distribution in a Virtual Water™ phantom. These parameters were chosen to match the absorbed dose calibration referenced parameters for clinical radiation beam standards to ensure acceptable accuracy and consistency in dosimetric data among institutions that provide radiation therapy and published literature. Energy fluence, percent depth dose and beam profile were calculated in a modeled phantom using MCNP. The calculated results were compared with measured reference data and showed good agreement for the photon spectrum.

---

* Varian Oncology Systems, Palo Alto, CA 94304 USA

CHAPTER 2

BACKGROUND

The MC technique involves using known probability distributions that govern the physical interactions of photons and electrons in various materials to simulate random trajectories of individual particles. By keeping track of processes of interest for a large number of histories, information regarding the average quantities and their correlated distributions can be obtained as well as the statistical fluctuations of specific events. The use of MC methods in radiation therapy physics has increased over the past few decades because the use of high energy photon and electron beams for radiotherapy has made it necessary to account for the electron transport for dosimetry and treatment planning purposes (Rogers and Bielajew, 1990).

2.1 Interactions of Radiation with Matter

In order to accurately simulate electron and photon transport, it is essential to correctly account for all the significant physical processes that occur. Thus, this section details the physical processes that affect simulation within the range of a few kilo-electron volts (keV) to tens of mega-electron volts (MeV).

2.1.1 Electron Interactions

Similar to other charged particles, electrons can both excite and ionize atoms by losing energy through collisions with atoms and molecules and can in turn be created as a byproduct of these collisions. Ionization occurs when a charged particle passes near an atom that exerts an electrical force on its orbital electrons strong enough to cause one of them to separate from the atom. The charged particle's lost energy is used to overcome

the orbital electron's binding energy and the remaining energy is used as kinetic energy for the ejected electron. If the ionization occurs within the inner shells of the atom characteristic x-rays or Auger electrons can be emitted. In addition, if the ejected electron is energetic enough it can cause secondary ionizations and is known as a delta ray.

Excitation occurs when the electron's encounter causes an atom's orbital electrons to be raised to a more excited state. The electron's energy loss is much smaller compared to ionization and the transferred energy is dissipated in the form of molecular vibrations, emission of infrared, visible, ultraviolet radiation and so forth (Cherry et al., 2003). Bremsstrahlung production occurs when a charged particle enters the electron cloud of an atom and strong electrical forces exerted by the atom's nucleus cause the particle to rapidly decelerate and lose energy which appears in the form of a photon of electromagnetic radiation. Figure 2.1 illustrates the primary electron interactions.

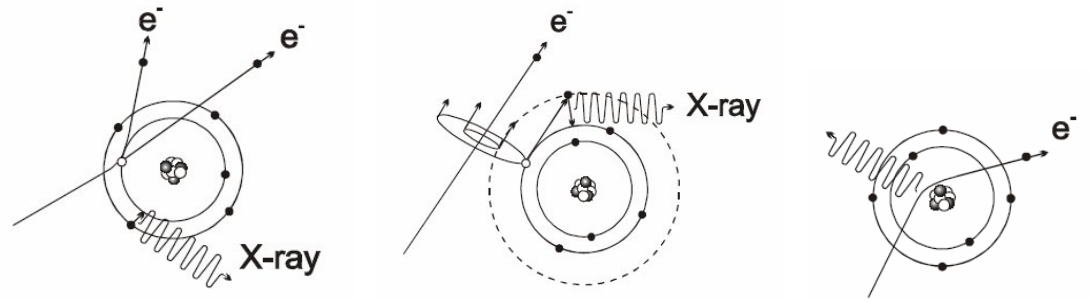

(a) (b) (c)

Figure 2.1: Primary Electron Interactions: (a) Ionization, (b) Excitation, and (c) Bremsstrahlung production (Miglierini, 2004)

Because electrons are much smaller for a given energy than heavier charged particles, their speeds are greater when passing through matter, making them more penetrating than heavy ions. In addition, electrons can lose a greater fraction of their energy in single collisions with other electrons as compared to heavy ions, resulting in an indeterminate range and a linear penetration distance unrelated to the actual path length through the medium. Electrons and positrons are thought of as continuously losing energy through inelastic collisions with bound atomic electrons and thus make electron transport using MC computations more complex and time-consuming than other particle transport calculations, such as photon transport.

2.1.2 Photon Interactions

A variety of interactions can occur when photons pass through matter. Unlike electrons, photons are considered secondary ionizing radiation because their interactions with atoms, nuclei and electrons do not directly cause ionization. Instead, they result in the ejection of orbital electrons or in the creation of positive-negative electron pairs, whose electrons cause ionization effects and are the basis for photon detection and radiation effects (Cherry et al., 2003). The three primary photon interactions are the photoelectric effect, Compton scattering and pair production; all of which, result in the ejection or creation of an electron.

The photoelectric effect dominates the lower gamma energies (a few hundred keV) where the incident photon energy is just enough to overcome the binding energy of orbital electron shells. It occurs when an atom fully absorbs the energy of an incident photon and utilizes the absorbed energy to eject an orbital electron whose energy is equivalent to the difference between the incident photon's energy and the binding energy

of the electron shell from which it was ejected. The vacancy in the electron shell then leads to the emission of characteristic x-rays or Auger electrons which undergo further electronic collisions contributing to the excitation and ionization of the matter in which it occurs.

Compton scattering, also known as incoherent scattering, is the process that governs interactions for photon energies on the order of 1 MeV and accounts for the majority of the medical physics range. It is essentially a collision between a higher (than the binding) energy photon and a loosely bound (or regarded as free) outer orbital atomic electron. The interaction results in a deflected photon of reduced energy and a recoil electron whose energy is dependent on the scattering angle. Rayleigh or coherent scattering occurs when the photon scatters elastically and a negligible amount of energy is lost.

For energies above a few MeV, pair production dominates the photon interactions. It occurs when a photon interacts with the electric field of a charged particle, usually an atomic nucleus and occasionally an electron, and creates an electron-positron pair who share the imparted kinetic energy: $E_{e+} + E_{e-} = E_o - 1.022$ MeV, where E_{e+} and E_{e-} are the energies of the resulting positron and electron respectively and E_o is the incident photon energy. Because the rest mass of an electron is 0.511 MeV the minimum incident photon energy required is 1.022 MeV and accounts for pair production's dominance of the higher photon energy range. The positron goes on to annihilate with an electron creating a pair of annihilation photons, 0.511 MeV in energy and approximately 180 degrees apart which cause further interactions. A much less common occurrence is when the photon interacts with the field of an atomic electron and

takes up a considerable amount of energy in the process and is thus referred to as triplet production and results in a vacancy left in the atom (Rogers and Bielajew, 1990). The primary photon interactions described above are schematically shown in Figure 2.2:

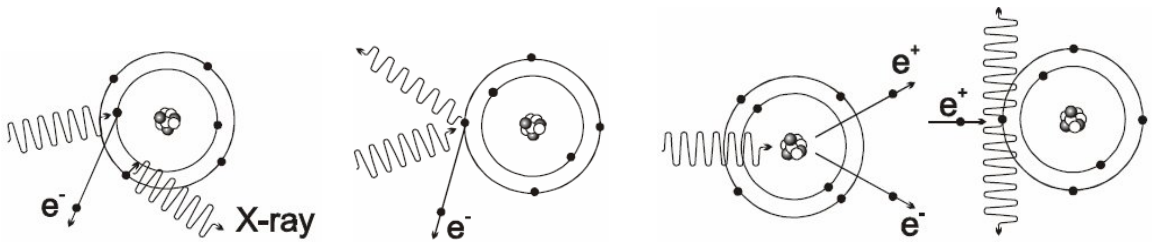

(a) (b) (c)

Figure 2.2: Primary Gamma-Ray Interactions: (a) Photoelectric effect, (b) Compton Scattering, and (c) Pair Production (Miglierini, 2004)

CHAPTER 3

METHODOLOGY

3.1 MCNP Methods

MCNP is a general purpose transport code that can be used for neutron, photon and electron or coupled particle transport. It has the capability of easily inputting complex geometry in three dimensions making the code very user friendly but at the cost of increased computation time. It has a wide range of capabilities for medical physics applications including, but not limited to, calculating dose, simulating radiographs, and creating voxel models using CT data (Goorley, 2005).

3.1.1 MCNP Runs and Techniques

MCNP automatically generates standard summary information for each simulation and gives the user better insight to the physics of the problem and the adequacy of the model, including: a complete account of the creation and loss of all tracks and their energies; the number of tracks entering, reentering and populating the cell; the number of collisions in a cell; the average weight, mean free path and energy of tracks in a cell; how the particles interacted with each nuclide in a cell; and a complete weight balance for each cell (MCNP – A General Monte Carlo N-Particle Transport Code, Version 5, 2003). In addition, MCNP provides basic tally types: six standard photon tallies and four standard electron tallies which can be easily modified for specific problems. The primary tallies used in this thesis are the surface current tally, F1, the track length estimate of cell flux, F4, the track length estimate of energy deposition, F6,

and the energy deposition tally, *F8. More information regarding these basic tallies and the underlying physics behind them can be found in the MCNP Version 5 User's Manual.

The latest available version of MCNP, MCNP5_1.3, offers several new useful features for medical physics applications. It has the capabilities of employing a 3D geometry independent tally grid for calculating volume averaged fluxes in voxels within the grid. In addition, other cards such as the tally multiplier FM card can be used with mesh tallies to calculate volume averaged doses and reaction rates. A brief mention of the other new applications include radiography tallies, photon Doppler broadening and an increase in number of detectors, tallies and particle histories used in a single run.

The MCNP runs designed in this thesis took place on a dual core AMD opteron 64 bit computer system running a Redhat Enterprise Linux ES Release 4.0 distribution composed of 17 nodes with 4 GB of ram. Despite the available computing power, the initial electron took approximately 70.6 hours when ran in parallel between 42 processors and subsequent runs took approximately 52 – 800 minutes on a single processor depending on the designated tallies.

3.2 Monte Carlo Modeling

Models have been said to generate new insights, provide basic understanding and give strong support to design, optimization and analysis of experiments (Siebert et al., 1997). Provided they are based on sound assumptions, accurate data, are carefully checked and appropriately applied within their scope, they can sometimes be used in lieu of experiments. In radiotherapy, models are created in order to predict dose distributions and are sometimes used as a substitution for measurements that are impractical in humans. For this purpose, the treatment head of a linac was modeled to determine the

spectral distribution of a 6 MV photon beam from a Varian 2100C along with a Virtual Water™ phantom and a human phantom model for future dose verification studies.

3.2.1 Modeling the Linear Accelerator

A linear accelerator uses high frequency electromagnetic waves to accelerate charged particles, such as electrons, to high energies through a linear tube in order to treat superficial tumors by utilizing the electron beam itself, or deep-seated tumors by making the electron beam strike a target to produce x-rays (Khan, 2003). The bremsstrahlung x-rays generated when electrons are incident on a high-Z target, such as tungsten, demonstrate a spectrum of x-ray energies with the maximum energy equal to the initial electron energy and with the average photon energy being approximately a third of the maximum energy.

Simulating the photon transport in the treatment head of a linac using MC methods allows for a reconstruction of the spectral photon data discussed above. In order to obtain a clinically applicable spectrum the major components of the treatment head must be accurately modeled. The primary components that affect the photon spectrum are the target composition, the primary collimator, which provides initial collimation of the beam directly following the target, the flattening filter, which allows for uniform beam intensity, and the upper and lower jaws, which allow for rectangular field size shaping and secondary collimation. Each of these components greatly affects the resulting photon spectrum and it is thus essential to accurately model them in order to properly characterize the beam for clinical applications.

An MCNP5 model was developed for the Varian Clinac 2100 based upon the manufacturer's specifications and previous documented literature (Mohan et al., 1985;

Fix et al., 2001; Cho et al., 2005). A 6.05 MeV electron beam with a radial distribution of 1mm was made to impinge on a tungsten target imbedded in copper. The electron transport and resulting x-ray production was simulated and tracked through the major components of the treatment head: the tungsten target, copper stopping plate, primary collimator and flattening filter. These components are responsible for the majority of photon attenuation within the treatment head

To avoid having to repeatedly run time consuming electron transport, a reusable surface source of the initial photon spectrum following the flattening filter was created for simplification and ease of subsequent runs. The reusable surface source was created utilizing a Surface Source Write (SSW) card which creates a surface source file by tracking and recording the particles (energy, position and angle) that cross a designated surface.

The first SSW card was created on the surface directly after the flattening filter and recorded the resulting bremsstrahlung production. The second SSW was written following the exit of the photons from the treatment head, not only to tally the photons that had made it past the jaws but also to make the incorporation of a multiple beam geometry and more complex phantom model easier for future calculations. This could be done by taking the second SSW and using it as a collimated planar beam source, 6 MV in energy, 10 x 10 cm^2 field, and with known distance from the surface of the object for which dose needs to be determined.

The visual schematic of the treatment head is pictured in Figure 3.1. The geometry and material composition of the various components within the linac treatment

head are based on the manufacturer's specifications and are under proprietary control (Varian Oncology Systems Monte Carlo Project, 1995-1996).

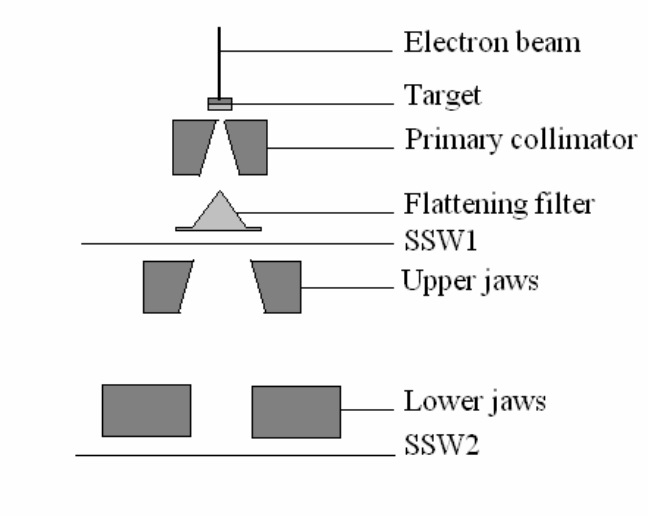

Figure 3.1: Schematic of Treatment Head

The jaws designated a 10cm x 10cm square field and the slab phantom was placed 100cm source-to-surface distance (SSD). The field size can be easily manipulated in the input file to create various field sizes, 10 x 10 cm^2 was chosen as a reference field for purposes of comparison to published data and for calibration of the linac for dosimetric calculations. Additionally, the beam could be rotated by translating the second SSW plane to incorporate different volumes for irradiation and this could in turn be used for multiple beam dose calculations. An illustration of the beam set up is shown in Figure 3.2.

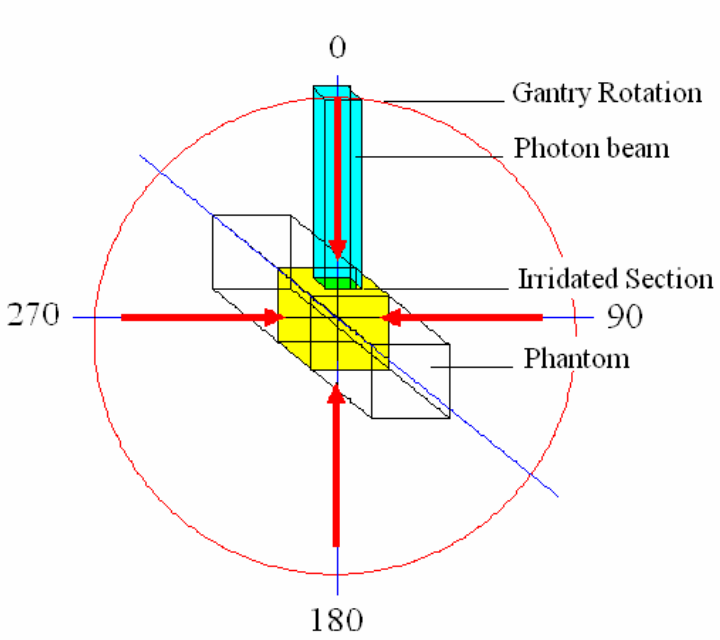

Figure 3.2: Schematic of Beam Set Up

3.2.2 Modeling Phantoms

For purposes of validating the x-ray spectra, a Virtual Water™ (VW) phantom was modeled and dose was determined within the slab phantom for comparison with measured data. Virtual Water™ phantoms are more convenient to work with than water phantom tanks during routine linear accelerator checks for photon and electron beam calibrations. They are designed to have layers of varying thickness to allow adjustable source-to-detector distances and to scatter and attenuate x-rays similarly to water within 0.5% equivalence without charge storage problems (Dosimetry Phantoms, Virtual Water™ Phantom Materials). The phantom modeled had dimensions 30 x 30 x 30cm^3 and was composed of epoxy resins and powders to control density and radiation properties. The specific material composition is 8.02% H, 67.03% C, 2.14% N, 19.91%

O, 0.14% Cl and 2.31% Ca by weight percent (Z. Wang et al.) with a density of 1.03g/cm^3.

Geometrically independent mesh tallies were created over the virtual water phantom, superimposing a cubic centimeter grid over the phantom in order to determine flux and energy of photons over the mesh cells. For the energy fluence mesh tally, 1 MeV energy bins were used from 0 to 6 MeV. This same technique could be applied to other phantom models for calculating dose in individual voxels to ensure optimization of dose.

In addition to modeling the VW phantom, a human phantom was modeled for future dose verification measurements. The Alderson Radiation Therapy (ART) male phantom 200A was modeled in MCNP5 utilizing Scan2MCNP, which converts CT, MRI and other scan data to an input file that can be used for Monte Carlo transport programs, such as MCNP, by constructing a 3D model from multiple digital communication (DICOM) files (Van Riper, 2003-2004). An original CT slice and its Scan2MCNP depiction are shown in Figure 3.2.

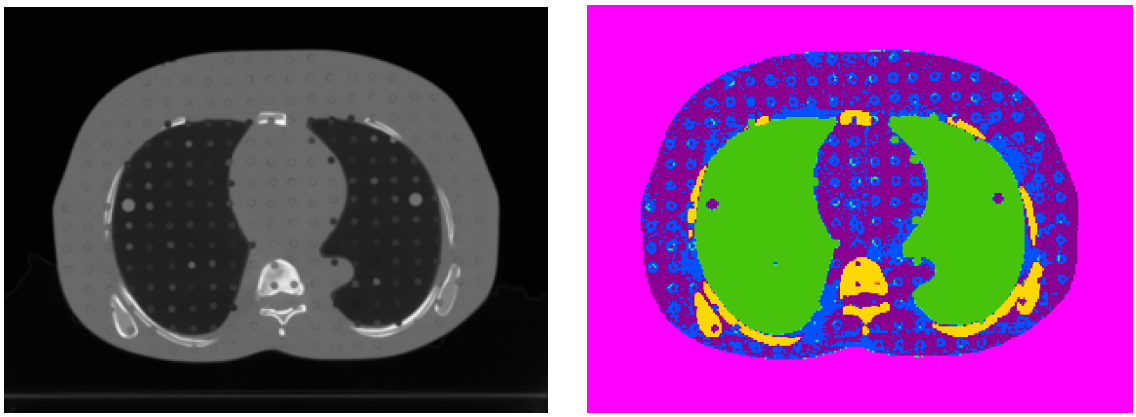

Figure 3.3: CT ART Slice and its Scan2MCNP Representation

A CT scan of the male ART phantom was taken at Emory University Hospital and converted into a 3D voxel phantom model using Scan2MCNP. The slices are modified by selecting the proper parameters to limit image artifacts and designating the appropriate colors to represent the different materials within the phantom. Further modifications can be made by directly altering the resulting output file. The MCNP5 model is pictured in Figure 3.4.

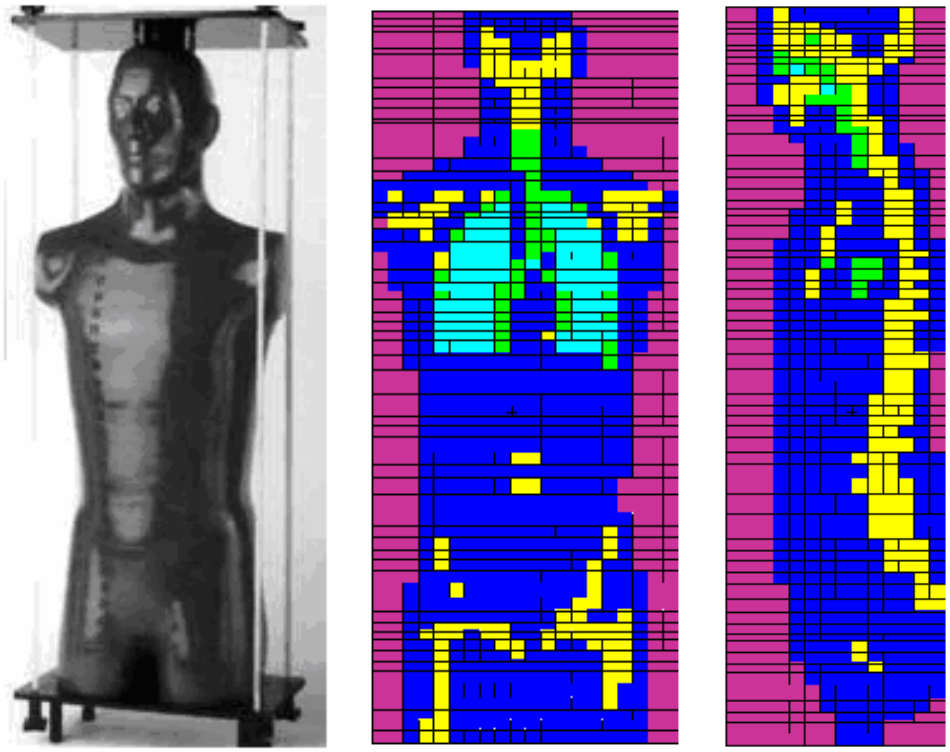

Figure 3.4: ART Phantom and MCNP5 VisEd Representation

The ART phantom is representative of a 175 cm (5 ft. 9 in.) tall, 73.5 kg (162 lb.) male and is made of ICRU-44 standard tissue-equivalent material (International Commission on Radiation Units and Measurements, 1989). The phantom is horizontally transected into 2.5cm slices containing hole grid 1.5 cm x 1.5 cm spacings with 5-7 mm

diameter holes for lung and tissue equivalent plugs for the use for thermo luminescent detector (TLD) chips and rods. The MCNP5 model consists of 3536 voxels and five materials which correspond to the colored partition boundaries shown in Table 3.1.

The materials are compositions from MIRD phantoms described in ORNL reports TM-8381 and TM-12907. Future work would include using the modeled ART phantom and conducting dose verification studies with various dosimetry methods for optimization purposes.

Table 3.1: MCNP5 Phantom Materials and Densities

Color	Material	Density (g/cm^3)
	Air @ 7200 ft	0.000987
	Adult Soft Tissues	1.040000
	Skeleton	1.400000
	Lung Tissue	0.296000
	Mixed Adult / Lung Tissues	0.605235

3.3 Dose Distributions

Absorbed dose, or simply dose, is defined as the mean energy imparted by ionizing radiation to a material of known mass. The standard unit of dose is the gray (Gy) and is equivalent to 100 radiation absorbed dose (rad). Linear accelerators are usually calibrated to deliver 1 cGy/Monitor Unit (MU). The MU is the linear accelerators deliverable dose unit and is used in medical physics calculations for determining dose to patients.

The majority of MCNP tallies are normalized to one starting source particle tying the tally normalization to the units of the source particle and how it is defined. Since peak target current and pulse width vary slightly from machine to machine due to accelerator tuning, the dose rate is based on repetition rates. Thus, making the quantity of

interest, the dose per pulse and for the target, the accumulated charge on the target per dose delivered. For the Varian 2100C 6 MV beam, the estimated mean energy incident on the target is approximately 6.4 MeV and an accumulated charge of approximately 11.2 μC will deliver 1 cGy absorbed dose to water for a 10 x 10cm^2 field, 100 cm SSD at a water depth of 1.6cm (dmax). In order to normalize an MCNP tally whose units are in MeV and determine absorbed dose the following equation (Goorley, 2005) would be used:

D(rads) = (*F8 tally (MeV) / source particle*mass (g))*(1.602x10-6 erg/MeV)*(1/100 erg/g/rad)*source particle

In radiation therapy, the absorbed dose of the incident beam varies with depth and depends on many parameters such as the beam energy, field size, SSD and the collimation system. Thus, measuring the depth dose variation along the central axis (CAX) of the beam is a fundamental step to calculating dose. One way to characterize the CAX dose distribution is to normalize the dose at depth with respect to a reference depth and this quantity is usually expressed as a percentage and is known as percent depth dose (PDD):

$$PDD = D_d/D_{do} * 100$$

D_d is the dose at depth, *d,* and D_{d0} is the dose at a fixed reference depth, *d0*, along the center of the beam. Usually, for lower energy x-rays the reference depth is at the

surface (*d0* = 0) and for higher energy x-rays the reference depth is taken at the depth of maximum dose, *dm* (*d0* = *dm*).

Dose was calculated in the VW phantom at various reference depths at the center of the 10 x 10 cm^2 field, in one centimeter diameter spheres using the *F8 tally (units of MeV/source particle) in MCNP5 and normalized to the reference dose maximum of 1.6 cm for a 6 MV photon beam. Comparative measurements were taken based on the clinical photon beam calibration protocol established by the American Association of Physicists in Medicine Task Group 51 (AAPM TG-51) for linacs and the tabulated data for the MCNP calculations and reference measurements can be found in the Appendix taken by Varian Oncology Associates using a Scanditronix Wellhoffer water phantom in one millimeter increments.

In addition to dose measurements, off-axis measurements were taken at d_{max} to plot a beam profile to determine the variation in dose across the field and to see the beam flatness, uniformity and alignment.

CHAPTER 4

RESULTS

4.1 Spectrum Calculations and Measurements

Table 4.1 shows the mean energy as a function of radial distance from the central axis (CAX). Mohan et al. demonstrated this technique, using annular rings to score the fluence and angular distribution of particles, for several beams of varying energies. He used annular rings of various radial distances from the CAX, 100 cm from the source in air and scored the different photon fluxes. These same parameters were used to determine the values shown in the Table below.

Table 4.1: Mean Energy as a Function of Radial Distance from the CAX

Radial Distance	Mean Energy (in MV)	Total error
0-2 cm	2.06	0.0053
2-3 cm	2.03	0.0047
3-5 cm	2.03	0.0026
5-10 cm	1.97	0.0012
10-15 cm	1.79	0.0021
15-20 cm	1.28	0.0058

As expected, the flattening filter hardens the beam more at the center of the beam than at the peripheral regions.

Figure 4.1 below illustrates that within a 0-2 cm circular diameter from the central axis (CAX) the photon spectrum has a distribution with higher energy photons and hence is harder compared with the spectrum in the annular region of 10-15cm from the CAX. The mean energy in the center or of the beam is 2.06 MeV and 1.79 MeV 10 to 15 cm from the central region.

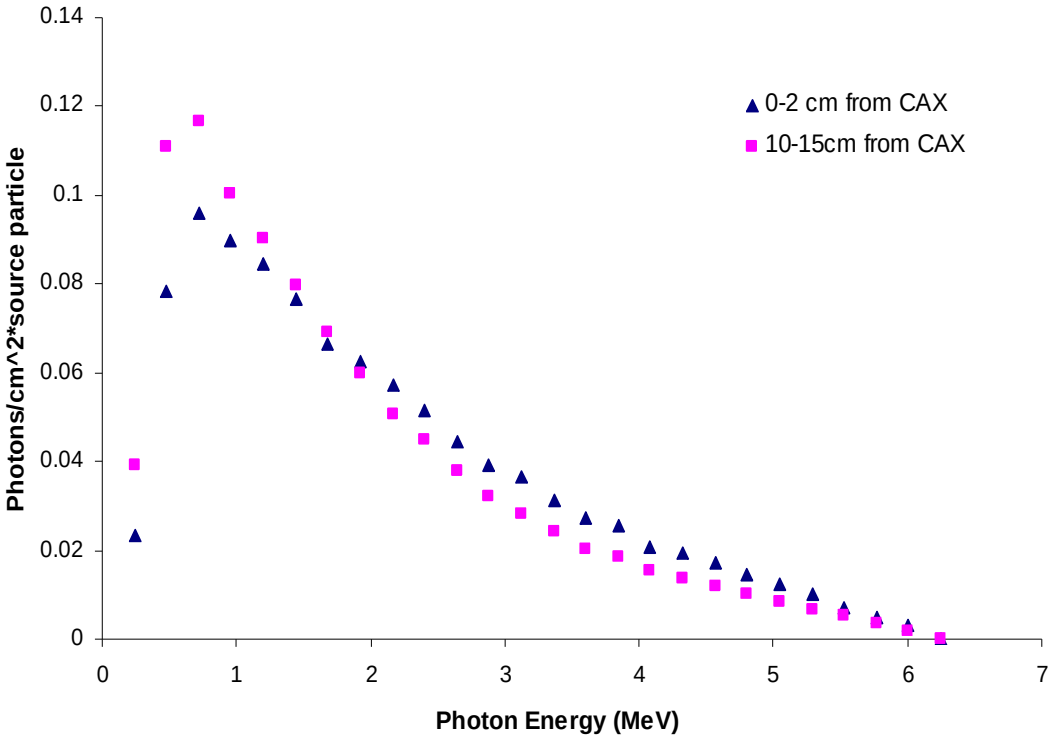

Figure 4.1: 6 MV photon spectra at varying radial distances

Because the region that most agreed with the referenced data was the spectrum from the 10-15cm radial ring, a surface source was created using the probability distribution from the MCNP tally to create a parallel beam for use in future calculations and the spectrum was verified through several runs using the same parameters as the measured data to ensure consistency.

The MCNP5 generated 6 MV photon spectrum is shown below in Figure 4.2. The photon flux was determined in a 1 cm diameter circle 100 cm source-to-surface distance (SSD) with a 10 x10 cm^2 field size, in air. Photons were scored in 0.25 MeV energy bins. The average energy of the overall x-ray spectrum was determined to be 1.79 MeV which agrees with the generally accepted value of approximately one third of the initial electron

energy. The standard deviation of the data is calculated from the fluctuations in the fluence data for each energy bin and was totaled to be 0.3%.

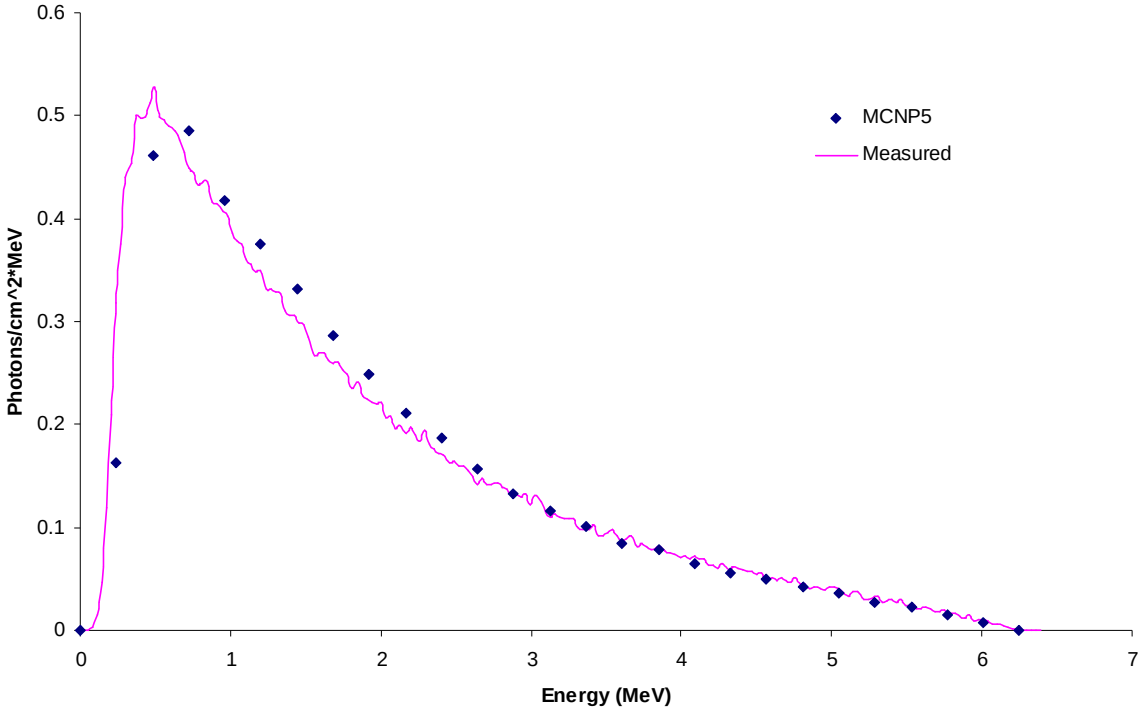

Figure 4.2: MCNP5 vs. Measured 6 MV Photon Spectrum

For purposes of comparison the spectrum from the Cho et al. paper of reference photon dosimetry data for the 6 MV Varian 2100C is show above. This spectrum was determined by studying the average data based on more than 50 sets of measured data from the Radiological Physics Center (RPC) and 10 sets of clinical dosimetry data obtained from 10 different institutions participating in a RPC study for quality assurance. The spectrum was measured in a 1 cm diameter circle, 100 cm SSD in a 10 x 102 field, in air. The measured spectrum's mean energy was determined to be 1.78 MeV. As can be seen above, the calculated and measured spectrums show good agreement.

Mesh tally results for the fluence were plotted in Gnuplot Version 4.0 (Williams, 2004) in Figure 4.3 below. The associated error of the flux tally is plotted above the photon fluence in the phantom to show that near the edges of the beam the fluence rate decreases rapidly, thus causing an increase in error as a function of the lateral distance of the beam. The fall off of the beam is caused both by the geometric penumbra and the reduced side-scatter. The bottom of graphs below, show their contours. A more accurate view of the contour map for the fluence mesh can be found in the appendix.

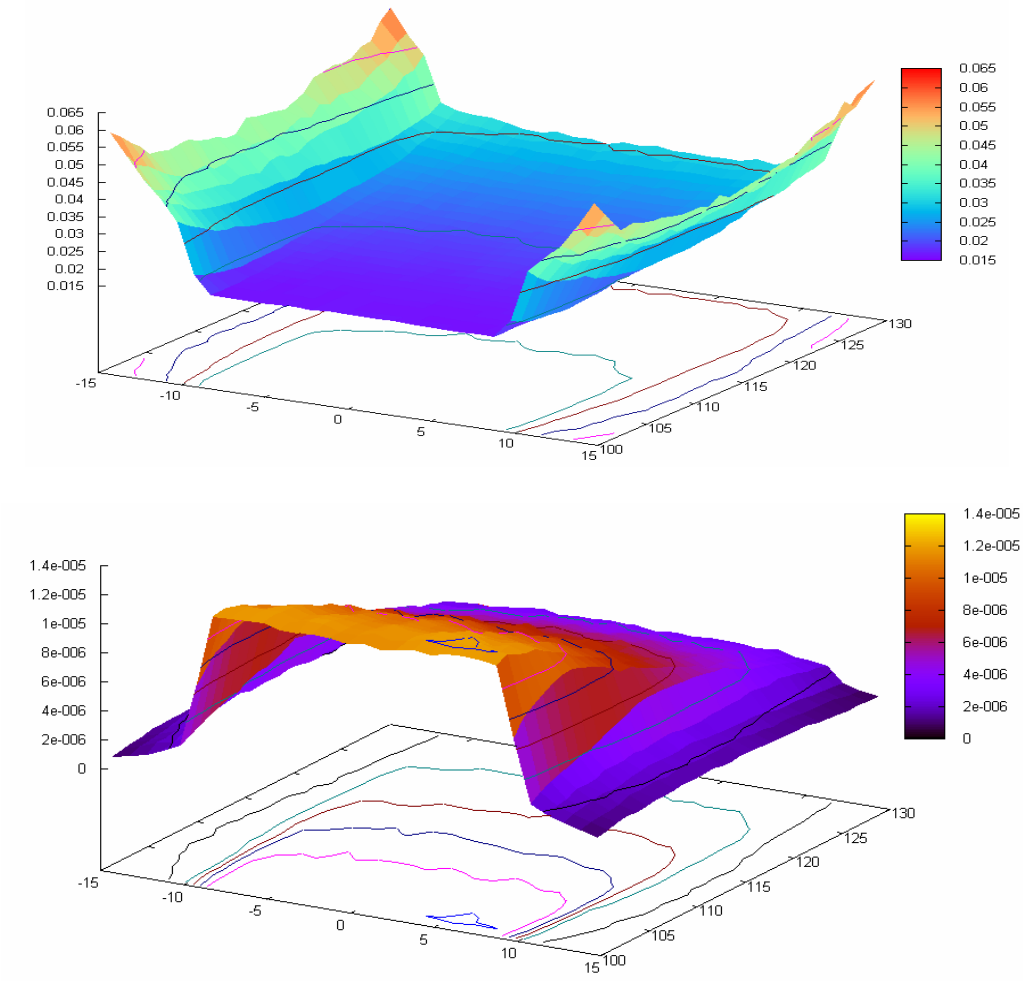

Figure 4.3: Flux mesh tally and corresponding error

Results for the energy fluence mesh tally for the various energy bins were plotted and can be found in the appendix. The 0 to 1 MeV energy mesh tally is plotted below in Figure 4.4. This plot shows that the majority of energy deposition is the result of the lower energy photons which agrees with the plotted 6 MV spectrum above which illustrates the modal energy within this range.

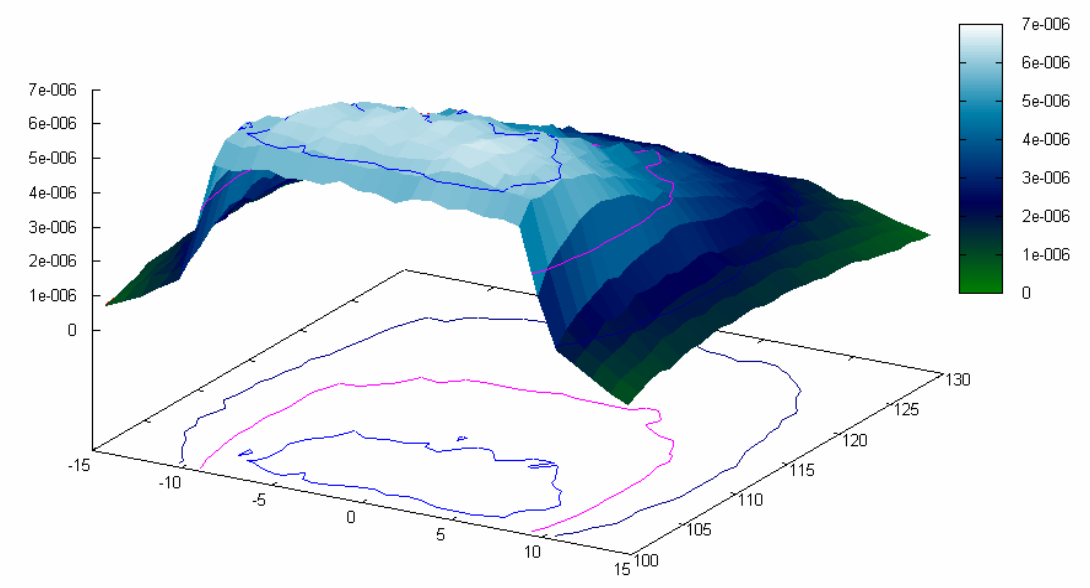

Figure 4.4: 0 to 1 MeV energy fluence mesh tally

4.1.1 Depth Dose Calculations and Measurements

Percent depth dose measurements were taken at various depths within the VW phantom and normalized to the referenced depth dose maximum, 1.6 cm, for a 6 MV photon beam 10 x 10 cm^2 field size, as illustrated in Figure 4.5.

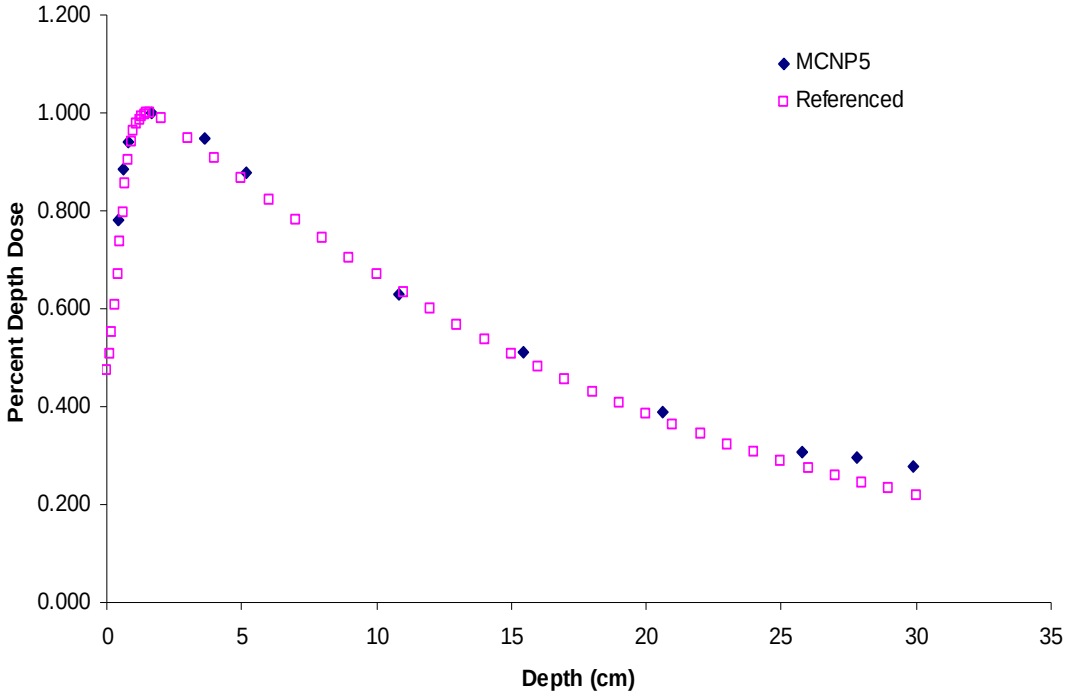

Figure 4.5: MCNP5 vs. Measured PDD for 6 MV beam

The MCNP5 calculated depth dose curve measurements were taken approximately every 5 cm except prior to the buildup region. The calculated results agreed fairly well with the referenced PDD curve, whose tabulated data can be found in the appendix. However, the referenced data obtained by Varian Oncology Associates was measured using an ionization chamber in a Wellhoffer Scanditronix water phantom in 1mm increments, thus the density differences between the referenced PDD values and those calculated in MCNP, are appropriately taken into account and there are slight visible differences between the two curves. In addition, the statistical error for the MCNP5 generated PDD curves are within 5% and it is assumed that the statistical error for the measured data is less than 2%.

The beam profile was determined at a depth of 1.6cm and is shown in Figure 4.6.

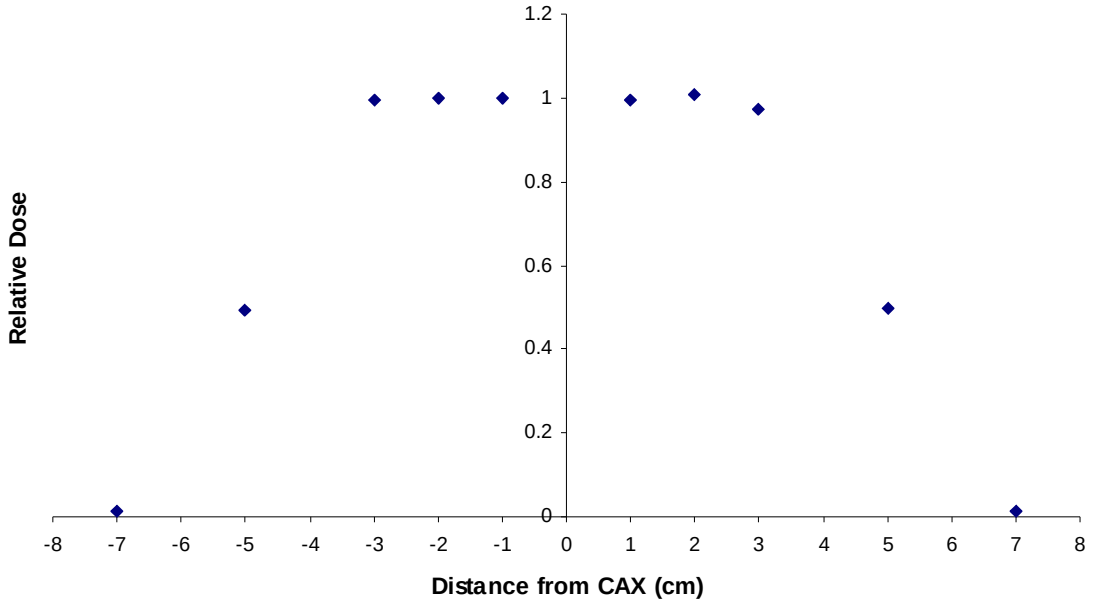

Figure 4.6: Beam profile for 6 MV beam

This figure shows the dose variation across the defined field at a specified depth. In addition, the beam profile conveys the beam flatness and the defined field size showing that the dose is uniform across the 10 x 10 cm^2 field. Thus, validating the correct geometry for the flattening filter and collimated jaws simultaneously.

CHAPTER 5

CONCLUSION

The 6 MV spectrum was successfully determined by the MC model as indicated in Figure 4.1, where the MCNP calculated spectrum is compared to a previously measured spectrum. In addition, the geometry of the treatment head, such as the flattening filter and collimating jaws, were sufficiently modeled. These results can be seen in the beam profile graph which shows that the flattening filter provided a uniform dose distribution across the field size and the expected beam hardening was graphed in the comparison of spectrums taken off the central axis. The PDD curves showed good agreement between the measured depth dose data and the calculated depth dose. A more conclusive calculation, however, with less statistical error and carried out in a water phantom as opposed to a VW phantom should be done prior to using the model for direct dose calculations in more complex phantoms.

The linac modeled in this paper can easily be changed to incorporate any number of geometries and sources encountered in medical physics. It has the ability to integrate different field sizes and nominal energies by simply changing a few values in the original input deck. This adaptability allows characterization of a number of different clinical photon beams, not just the 6 MV beam; current modern day linear accelerators typically have more than one operating photon energy. Presently, this model can create multiple 6 MV beam setups similar to the standard prostate radiation therapy treatment of placing a beam at every 90 degrees (AP/PA) and of course single 6 MV beam data can be determined as well.

CHAPTER 6

FUTURE WORK

The methods used in this work were designed to model the 6 MV photon beam of a Varian 2100C and to analyze and validate the resulting spectrum using dose distribution measurements in a VW phantom. However, several assumptions and simplifications were made regarding the calculations and experimental measurements within the Virtual Water^{TM} phantom. Depth dose measurements were tallied directly in the VW phantom material and normalized to determine the dose distribution, thus future work would include modeling an ionization chamber in MCNP for dose calculations in the phantom.

In addition, future research would include measurements and dose distributions in more complex phantom models such as the ART phantom using varying methods of dosimetry, such as film and TLDs to validate dose. The linac model could be modified to simulate more complex beam shapes by properly modeling the multi-leaf collimators in order to accommodate irregular field shapes to make the beam model more patient specific and practical for clinical purposes. This could lead to Image Modulated Radiation Therapy (IMRT) techniques by creating multiple beam setups using MLC shaping and eventually dose optimization.

Besides adding more complex geometry into the MC problem, modeling the ionization chamber, MLC, human phantoms and multiple beam treatments, it would be beneficial to explore other MC codes. Determining the similarities and differences for each code would convey their strengths and weaknesses and allow efficient use of their strengths for specific radiation therapy problems to be applied. Also, exploring the different types of radiation used for treatment, such as electron, proton and neutron beams is also a possibility.

Finally, it is apparent that technology is continuously getting more complex to adapt to patient specific treatments in the field of medical physics, i.e. image gating to take into account the movement of the patients organs during inhalation and exhalation. Thus, MC modeling and development of calculation algorithms will also be continually changing and researched in order to accommodate the needs for better dose distribution and optimization in radiation therapy. Steady, ongoing research is presently being carried out in all these areas to reach the common goal of a radiation therapy; maximum dose to the tumor volume and minimal dose to the healthy/surrounding tissue and thus a better quality of life for patients.

APPENDIX A

REFERENCED DATA AND TABULATED RESULTS

Table A.1: Referenced Spectrum Data for 6 MV Spectrum (Cho et al., 2005)

energy	probability	error
0.016027	7.40E-09	7.40E-09
0.048082	3.80E-09	2.20E-09
0.080137	5.67E-08	1.58E-08
0.11219	3.09E-07	3.53E-08
0.14425	9.36E-07	6.37E-08
0.1763	2.38E-06	9.08E-08
0.20836	4.20E-06	1.12E-07
0.24041	6.36E-06	1.37E-07
0.27247	7.51E-06	1.45E-07
0.30452	8.79E-06	1.57E-07
0.33658	9.06E-06	1.55E-07
0.36863	1.00E-05	1.65E-07
0.40069	9.94E-06	1.62E-07
0.43274	9.99E-06	1.61E-07
0.4648	1.03E-05	1.63E-07
0.49685	1.06E-05	1.69E-07
0.52891	9.99E-06	1.58E-07
0.56096	9.92E-06	1.57E-07
0.59302	9.79E-06	1.55E-07
0.62507	9.72E-06	1.57E-07
0.65713	9.52E-06	1.56E-07
0.68918	9.30E-06	1.50E-07
0.72124	9.00E-06	1.48E-07
0.75329	8.89E-06	1.45E-07
0.78535	8.64E-06	1.42E-07
0.8174	8.72E-06	1.46E-07
0.84946	8.72E-06	1.48E-07
0.88151	8.32E-06	1.42E-07
0.91357	8.29E-06	1.43E-07
0.94562	8.13E-06	1.37E-07
0.97768	8.06E-06	1.40E-07
1.0097	7.72E-06	1.38E-07
1.0418	7.58E-06	1.33E-07
1.0738	7.50E-06	1.31E-07
1.1059	7.19E-06	1.30E-07
1.138	7.12E-06	1.28E-07
1.17	6.96E-06	1.29E-07
1.2021	6.99E-06	1.28E-07
1.2341	6.64E-06	1.21E-07
1.2662	6.62E-06	1.24E-07
1.2982	6.57E-06	1.23E-07
1.3303	6.55E-06	1.25E-07
1.3623	6.21E-06	1.20E-07
1.3944	6.12E-06	1.20E-07
1.4264	6.13E-06	1.19E-07
1.4585	5.96E-06	1.17E-07
1.4906	5.93E-06	1.17E-07
1.5226	5.69E-06	1.13E-07
1.5547	5.33E-06	1.08E-07
1.5867	5.38E-06	1.08E-07
1.6188	5.38E-06	1.11E-07
1.6508	5.25E-06	1.08E-07
1.6829	5.18E-06	1.06E-07
1.7149	5.20E-06	1.09E-07
1.747	5.06E-06	1.08E-07
1.7791	4.98E-06	1.05E-07
1.8111	4.69E-06	1.02E-07
1.8432	4.81E-06	1.06E-07
1.8752	4.56E-06	1.01E-07
1.9073	4.51E-06	9.79E-08
1.9393	4.44E-06	1.01E-07
1.9714	4.40E-06	1.01E-07
2.0034	4.42E-06	9.91E-08
2.0355	4.14E-06	9.19E-08
2.0675	4.15E-06	9.61E-08
2.0996	3.91E-06	9.01E-08
2.1317	3.99E-06	9.20E-08
2.1637	3.83E-06	9.05E-08
2.1958	3.95E-06	9.47E-08
2.2278	3.79E-06	9.12E-08
2.2599	3.69E-06	9.03E-08
2.2919	3.88E-06	9.41E-08
2.324	3.63E-06	8.55E-08
2.356	3.53E-06	8.93E-08
2.3881	3.45E-06	8.44E-08
2.4202	3.41E-06	8.51E-08
2.4522	3.25E-06	8.51E-08
2.4843	3.29E-06	8.41E-08
2.5163	3.18E-06	8.02E-08
2.5484	3.19E-06	8.33E-08
2.5804	3.10E-06	8.02E-08
2.6125	3.00E-06	7.74E-08
2.6445	2.83E-06	7.46E-08
2.6766	2.95E-06	7.51E-08
2.7086	2.83E-06	7.58E-08
2.7407	2.82E-06	7.62E-08
2.7728	2.87E-06	7.85E-08
2.8048	2.77E-06	7.70E-08
2.8369	2.74E-06	7.48E-08

Table A.1: Referenced Spectrum Data for 6 MV Spectrum continued (Cho et al., 2005)

2.8689	2.63E-06	7.14E-08
2.901	2.66E-06	7.69E-08
2.933	2.58E-06	7.14E-08
2.9651	2.65E-06	7.59E-08
2.9971	2.44E-06	6.86E-08
3.0292	2.62E-06	7.64E-08
3.0613	2.50E-06	7.50E-08
3.0933	2.29E-06	6.50E-08
3.1254	2.20E-06	6.48E-08
3.1574	2.26E-06	6.81E-08
3.1895	2.20E-06	6.59E-08
3.2215	2.16E-06	6.38E-08
3.2536	2.19E-06	6.70E-08
3.2856	2.17E-06	6.56E-08
3.3177	1.99E-06	5.83E-08
3.3497	1.96E-06	5.89E-08
3.3818	1.97E-06	6.22E-08
3.4139	2.06E-06	6.60E-08
3.4459	1.85E-06	6.16E-08
3.478	1.84E-06	6.05E-08
3.51	1.91E-06	6.04E-08
3.5421	1.96E-06	6.28E-08
3.5741	1.84E-06	6.04E-08
3.6062	1.75E-06	5.78E-08
3.6382	1.77E-06	6.01E-08
3.6703	1.83E-06	6.06E-08
3.7024	1.64E-06	5.15E-08
3.7344	1.68E-06	5.78E-08
3.7665	1.64E-06	5.64E-08
3.7985	1.58E-06	5.31E-08
3.8306	1.59E-06	5.43E-08
3.8626	1.64E-06	5.64E-08
3.8947	1.53E-06	5.29E-08
3.9267	1.52E-06	5.34E-08
3.9588	1.47E-06	5.15E-08
3.9908	1.43E-06	4.92E-08
4.0229	1.45E-06	5.08E-08
4.055	1.40E-06	4.91E-08
4.087	1.44E-06	5.13E-08
4.1191	1.39E-06	5.24E-08
4.1511	1.40E-06	5.17E-08
4.1832	1.27E-06	4.85E-08
4.2152	1.28E-06	4.84E-08
4.2473	1.22E-06	4.84E-08
4.2793	1.29E-06	4.93E-08
4.3114	1.17E-06	4.46E-08
4.3435	1.25E-06	4.74E-08
4.3755	1.21E-06	4.75E-08
4.4076	1.18E-06	4.63E-08
4.4396	1.16E-06	4.66E-08
4.4717	1.13E-06	4.55E-08
4.5037	1.10E-06	4.54E-08
4.5358	1.12E-06	4.44E-08
4.5678	1.01E-06	4.05E-08
4.5999	1.04E-06	4.30E-08
4.6319	9.57E-07	4.04E-08
4.664	1.04E-06	4.32E-08
4.6961	9.74E-07	3.95E-08
4.7281	9.26E-07	3.62E-08
4.7602	1.03E-06	4.59E-08
4.7922	9.18E-07	3.91E-08
4.8243	8.96E-07	4.09E-08
4.8563	8.15E-07	3.70E-08
4.8884	8.47E-07	3.79E-08
4.9204	8.08E-07	3.71E-08
4.9525	7.88E-07	3.66E-08
4.9846	8.45E-07	3.93E-08
5.0166	8.41E-07	3.84E-08
5.0487	8.05E-07	3.87E-08
5.0807	7.12E-07	3.32E-08
5.1128	6.61E-07	3.27E-08
5.1448	7.45E-07	3.60E-08
5.1769	7.43E-07	3.67E-08
5.2089	6.11E-07	3.02E-08
5.241	5.89E-07	3.01E-08
5.273	6.25E-07	3.33E-08
5.3051	6.74E-07	3.71E-08
5.3372	5.52E-07	2.93E-08
5.3692	5.70E-07	3.00E-08
5.4013	6.00E-07	3.28E-08
5.4333	5.44E-07	2.99E-08
5.4654	6.00E-07	3.19E-08
5.4974	4.72E-07	2.66E-08
5.5295	5.17E-07	2.87E-08

Table A.1: Referenced Spectrum Data for 6 MV Spectrum continued (Cho et al., 2005)

5.5615	4.31E-07	2.55E-08
5.5936	4.28E-07	2.60E-08
5.6257	4.48E-07	3.03E-08
5.6577	4.19E-07	2.71E-08
5.6898	3.76E-07	2.75E-08
5.7218	3.65E-07	2.22E-08
5.7539	3.94E-07	2.82E-08
5.7859	3.29E-07	2.44E-08
5.818	3.29E-07	2.44E-08
5.85	2.75E-07	2.16E-08
5.8821	2.54E-07	2.04E-08
5.9141	2.91E-07	2.45E-08
5.9462	1.89E-07	1.54E-08
5.9783	2.08E-07	1.87E-08
6.0103	2.04E-07	1.87E-08
6.0424	1.70E-07	1.85E-08
6.0744	1.32E-07	1.35E-08
6.1065	1.20E-07	1.39E-08
6.1385	7.99E-08	1.18E-08
6.1706	7.10E-08	1.02E-08
6.2026	3.62E-08	7.43E-09
6.2347	2.65E-08	5.92E-09
6.2668	9.76E-09	4.01E-09
6.2988	4.74E-09	2.16E-09
6.3309	1.80E-09	1.30E-09
6.3629	3.01E-09	1.77E-09
6.395	1.08E-09	1.08E-09

Figure A.1: 6 MV Open Field Percentage Depth Doses (Varian Oncology Systems)

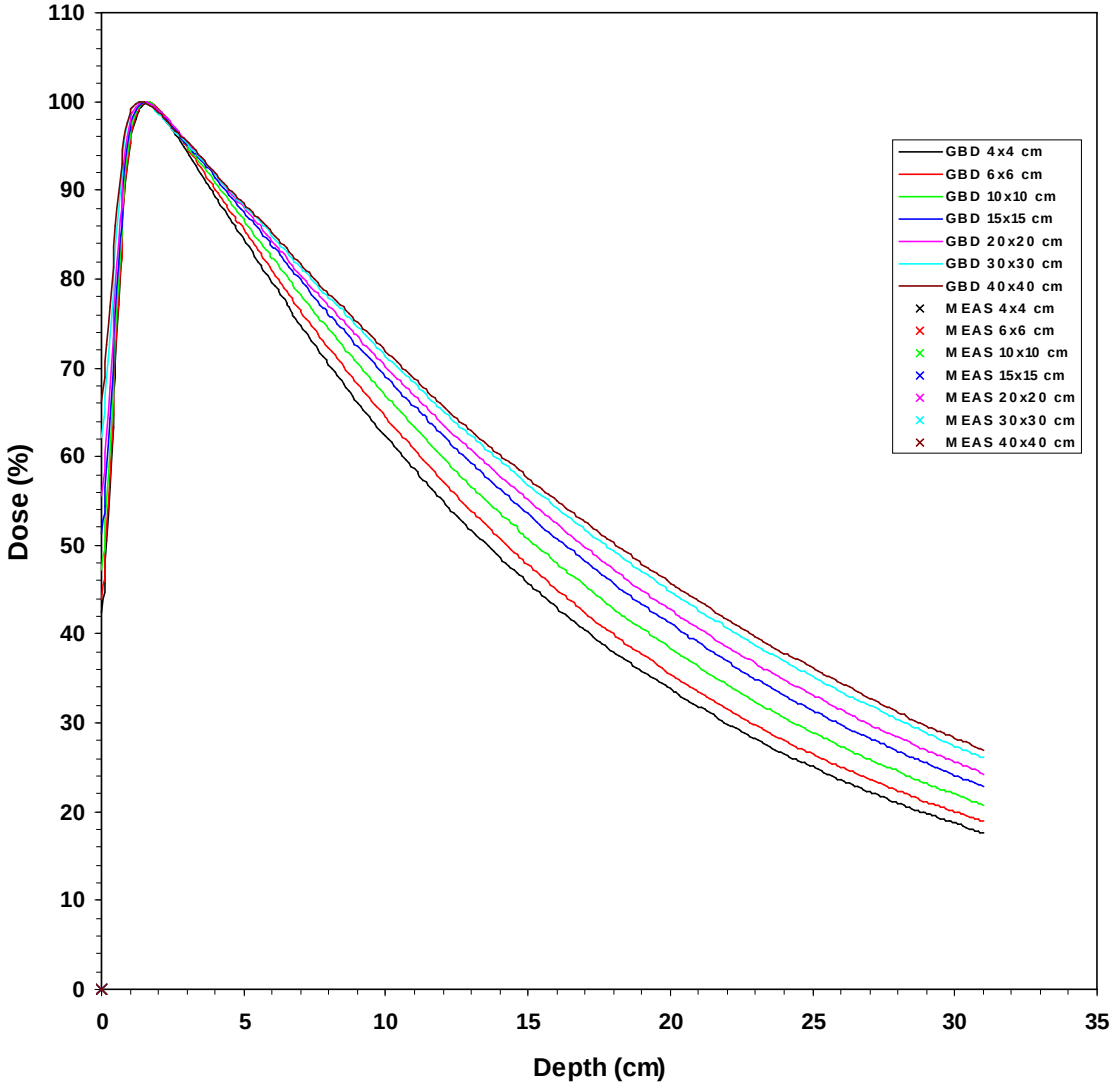

Table A.2: 6 MV, 10 x 10 cm^2 Field Percent Depth Doses (Varian Oncology Systems)

Depth (cm)	PDD
0.0	0.473
0.1	0.506
0.2	0.552
0.3	0.609
0.4	0.672
0.5	0.738
0.6	0.796
0.7	0.855
0.8	0.904
0.9	0.94
1.0	0.963
1.1	0.976
1.2	0.987
1.3	0.994
1.4	0.998
1.5	0.999
1.6	1
2.0	0.99
3.0	0.95
4.0	0.909
5.0	0.867
6.0	0.824
7.0	0.782
8.0	0.743
9.0	0.704
10.0	0.669
11.0	0.634
12.0	0.599
13.0	0.566
14.0	0.537
15.0	0.507
16.0	0.48
17.0	0.455
18.0	0.428
19.0	0.406
20.0	0.384
21.0	0.364
22.0	0.343
23.0	0.324
24.0	0.306
25.0	0.289
26.0	0.274
27.0	0.259
28.0	0.245
29.0	0.232
30.0	0.22

Table A.3: Beam Profile Measurements Using MCNP

distance from CAX (cm)	MeV/source particle	error	arbitrary units
7	1.420860E-06	0.0202	0.011470111
5	6.139010E-05	0.012	0.495581029
3	1.207580E-04	0.0086	0.974837538
2	1.247140E-04	0.0085	1.006772957
1	1.234890E-04	0.0085	0.996883956
-1	1.237300E-04	0.0085	0.998829465
-2	1.238750E-04	0.0085	1
-3	1.231930E-04	0.0085	0.99449445
-5	6.126200E-05	0.012	0.494546922
-7	1.429940E-06	0.0202	0.011543411

REFERENCES

American Cancer Society. "Cancer Facts and Figures 2006." http://www.cancer.org/docroot/STT/stt_0.asp (Accessed April 6, 2006).

Andreo, P., Monte Carlo techniques in medical radiation Physics. Physics in Medicine and Biology. 1990, 36, 861-920.

Cherry, Simon R., James A. Sorenson, Michael E. Phelps. Physics in Nuclear Medicine, Third Edition. Saunders, Philadelphia. 2003.

Cho, Sang Hyun, Oleg N. Vassiliev, Seungsoo Lee, H. Helen Liu, Geoffrey S. Ibbott, and Radhe Mohan, Reference photon dosimetry data and reference phase space data for the 6 MV photon beam from Varian Clinac 2100 Series linear accelerators. Medical Physics. 2005, 32(1), 137-148.

Ding, George X., Energy spectra, angular spread, fluence profiles and dose distributions of 6 and 18 MV photon beams: results of Monte Carlo simulations for Varian 2100EX accelerator. Physics in Medicine and Biology. 2002, 47, 1025-1046.

Dosimetry Phantoms, "Virtual Water™ Phantom Materials," CNMC Company. http://www.cnmcco.com/products/Virtual%20Water.pdf (Accessed April 4, 2006).

Fix, Michael K., Marco Stampanoni, Peter Manser, Ernst J Born, Roberto Mini and Peter Rüegsegger, A multiple source model for 6 MV photon beam dose calculations using Monte Carlo. Physics in Medicine and Biology. 2001, 46, 1407-1427.

Goorley, Tim and Dick Olsher, Using MCNP5 for Medical Physics Applications. American Nuclear Society Topical Meeting – Monte Carlo 2005. Chattanooga, TN, USA. April 17-21, 2005.

Karzmark, C. J. and Robert J. Morton. A Primer on Theory and Operation of Linear Accelerators in Radiation Therapy. Medical Physics Publishing, Madison. 1998.

International Commission on Radiation Units and Measurements, "Tissue Substitutes in Radiation Dosimetry and Measurement." ICRU Report 44 (1998).

J. F. B. (Editor), MCNP – A General Monte Carlo N-particle transport code, Los Alamos National Laboratory Report LA-12625-M. Los Alamos, NM, 1993.

Kawano, T. "Gnuplot – not so frequently asked questions." 2004-2005, http://t16web.lanl.gov/Kawano/gnuplot/index-e.html (Accessed April 4, 2006).

Keall, Paul J., Jeffrey V. Siebers, Bruce Libby and Radhe Mohan, Determining the incident electron fluence for Monte Carlo-based photon treatment planning using a standard measured data set. Medical Physics. 2003, 30(4), 574-582.

Khan, Faiz M. The Physics of Radiation Therapy, Third Edition. Lippincott Williams & Wilkins, Philadelphia. 2003.

Ma, Chang-Ming and Steve B Jiang, Monte Carlo modeling of electron beams from medical accelerators. Physics in Medicine and Biology. 1999, 44, R157-R189.

Ma, Chang-Ming, Characterization of computer simulated radiotherapy beams for Monte-Carlo treatment planning. Radiation Physics and Chemistry. 1998, 53, 329-344.

Mackie, T. R., Applications of the Monte Carlo Method in Radiotherapy, in Vol. III of "Dosimetry of Ionization Radiation" eds. K. Kase, B. Bjärngard and F. H. Attix. Academic Press, New York. 1990, 541-620.

Miglierini, Marcel. "Detectors of Radiation." Wigner Course on Reactor Physics Experiments. Bratislava, Slovakia. 27 April – 15 May 2004, http://www.reak.bme.hu/nti/Education/Wigner_Course/2004/WignerManuals/Bratislava/detectors.pdf (Accessed October 11, 2005).

Mohan, Radhe and Chen Chui, Energy and angular distributions of photons from medical linear accelerators. Medical Physics. 1985, 12(5), 592-597.

Rogers, D. W. O., Monte Carlo Techniques in Radiotherapy. Physics in Canada, Medical Physics Special Issue. 2002, 58(2), 63-70.

Rogers, D. W. O. and A. F. Bielajew, Monte Carlo Techniques of Electron and Photon Transport for Radiation Dosimetry, in Vol. III of "Dosimetry of Ionization Radiation" eds. K. Kase, B. Bjärngard and F. H. Attix. Academic Press, New York. 1990, 427-539.

Siebert, B. R. L. and R. H. Thomas, Computational Dosimetry. Radiation Protection Dosimetry. 1997, 70(1-4), 371-378.

Siebers, J. V., P. J. Keall, B. Libby and R. Mohan, Comparison of EGS4 and MCNP4b Monte Carlo codes for generation of photon phase space distributions for a Varian 2100C. Physics in Medicine and Biology. 1999, 44, 3009-3026.

Van Riper, K. A. Scan2MCNP User Manual: CT & MRI Scan Data to MCNP Input Format Conversion Software. White Rock Science, 2003-2004.

Varian Oncology Systems Monte Carlo Project Confidential Information. Monte Carlo Package, 1995-1996.

Vassiliev, Oleg N., Uwe Titt, Stephen F. Kry, Falk Pönisch, Michael T. Gillin and Radhe Mohan, Monte Carlo study of photon fields from a flattening filter-free clinical accelerator. Medical Physics. 2006, 33(4), 820-827.

Verhaegen, Frank and Jan Seuntjens, Monte Carlo modeling of external radiotherapy photon beams. Physics in Medicine and Biology. 2003, 48, R107-R164.

Wang, Zhonglu and Nolan E. Hertel, Determination of dosimetric characteristics of OptiSeed^{TM} a plastic brachytherapy ^{103}Pd source. Applied Radiation and Isotopes. 2005, 63, 311-321.

Williams, Thomas and Colin Kelley. Gnuplot, An Interactive Plotting Program Version 4.0. 1986-1993, 1998, 2004.

X-5 Monte Carlo Team. MCNP – A General Monte Carlo N-Particle Transport Code, Version 5 manual. 2003.